lower freezing point of N_2 relative to argon, and hence a slightly slower rate of freezing during the deposition process and slightly greater mobility of the reactant species. It is also interesting to note that a recent study[24] of the SO_2/H_2O system found the large majority of the sulfur either in the form of SO_2 or as $S_2O_5^{2-}$, while very little of the intermediate SO_3^{2-} was noted.

The disulfite $S_2O_5^{2-}$ anion might form by one of several routes under these conditions. One is the simultaneous, three-body collision of two SO_2 molecules and Tl_2O, but this is quite unlikely at the concentrations employed. More likely, formation of $S_2O_5^{2-}$ involves initial formation of the SO_3^{2-} anion, followed by addition of a second SO_2 unit to form the final product anion. The fact that the ^{18}O label appears in the bridging position as well as in the terminal oxygen positions is consistent with this view as well. If this is the mechanism by which $S_2O_5^{2-}$ is formed, then the addition of SO_2 to SO_3^{2-} must be very facile, with effectively no activation energy, since in many cases nearly all of the SO_3^{2-} is converted to $S_2O_5^{2-}$ during the condensation process. A final possible mechanism, the reaction of Tl_2O with sulfur dioxide dimer, $(SO_2)_2$, cannot be ruled out but does not seem likely in that this dimer is weakly bound and should not be abundant at the concentrations employed.

Conclusions

The reaction of thallium(I) oxide, Tl_2O, with SO_2 under matrix isolation conditions has given rise to two distinct product species, the SO_3^{2-} and $S_2O_5^{2-}$ anions, each in a triple ion with two Tl^+ cations. The infrared spectrum of the $Tl^+_2SO_3^{2-}$ species showed a lowering of the SO_3^{2-} symmetry due to ion pairing, in a manner similar to that for the $M^+ClO_3^-$ ion pairs. The infrared spectrum of $S_2O_5^{2-}$ indicated an oxygen-bridged structure under these conditions, rather than the unsymmetrical S–S linkage found for the room-temperature, crystalline material. Finally, further evidence has been obtained to support the utility of the oxide salt/molecule technique in forming and isolating oxygen-containing anions that either decompose upon vaporization or are not stable under room-temperature conditions.

Acknowledgment. The authors gratefully acknowledge support of this research by the National Science Foundation, through Grant CHE 81-00119. B.S.A. also gratefully acknowledges the Dreyfus Foundation for a Teacher-Scholar grant.

Registry No. Tl_2O, 1314-12-1; SO_2, 7446-09-5; Tl_2SO_3, 13453-46-8; $S_2O_5^{2-}$, 23134-05-6; ^{18}O, 14797-71-8.

Contribution from the Corporate Research Science Laboratories, Exxon Research and Engineering Company, Annandale, New Jersey 08801

EXAFS Studies of Amorphous Molybdenum and Tungsten Trisulfides and Triselenides

S. P. CRAMER,* K. S. LIANG, A. J. JACOBSON, C. H. CHANG, and R. R. CHIANELLI

Received July 21, 1983

The structure of the amorphous molybdenum and tungsten trisulfides and triselenides has been investigated by using X-ray absorption spectroscopy. Analysis of the metal EXAFS data revealed metal–metal distances between 2.74 and 2.79 Å, as well as normal, but disordered, metal–chalcogen distances (Mo–S = 2.44 Å, W–S = 2.41 Å, Mo–Se = 2.53 Å, W–Se = 2.55 Å). The selenium EXAFS of the triselenides shows Se–Se distances of 2.35–2.37 Å. It is proposed that the important structural unit of these amorphous materials is a binuclear metal site with a triple bridge consisting of one chalcide ion and one dichalcide ion. Several results of general applicability for EXAFS analysis were obtained during the course of this work. Procedures using experimental amplitude functions have been developed that yield meaningful estimates of static disorder. The utility of curve-fitting procedures for L_{III} edge EXAFS analysis has also been demonstrated, and screening effects on second-shell EXAFS amplitudes have been quantified.

Introduction

The amorphous trichalcides MoS_3, WS_3, $MoSe_3$, and WSe_3 have interesting electrochemical and physical properties.[1] They are normally prepared by thermal decomposition of the corresponding diammonium tetrachalcidometalate salts,[2] although similar materials can be made by solution procedures.[3] X-ray diffraction analysis shows that the trichalcides prepared by either method are amorphous in nature,[4-6] a property that has hindered their characterization on an atomic scale. Stimulated in part by the fact that MoS_3 can be used as a cathode material to construct a high-energy-density alkali-metal battery,[1] the structural characterization of these materials by a variety of methods has been undertaken.[6,7] In this paper, the outcome of an X-ray absorption study of these materials is reported. The EXAFS (extended X-ray absorption fine structure) data, interpreted by comparison with the corresponding crystalline $(NH_4)_2MX_4$ and MX_2 compounds, clearly demonstrate metal–metal bonding in all of the MX_3 materials examined, with metal–metal bond lengths shorter than those previously suggested by X-ray radial distribution function analysis.[5]

Several advances in the experimental approach to the analysis of EXAFS data were achieved in the course of this work. First, it is shown that reliable Debye–Waller factors can be obtained by the combination of vibrational normal-mode calculations and curve-fitting techniques and that these factors are useful for interpreting the EXAFS of amorphous materials. It has also been shown that these techniques are applicable to L_{III} edges as well as K edges. Finally, there has

(1) Jacobson, A. J.; Chianelli, R. R.; Rich, S. M.; Whittingham, M. S. *Mater. Res. Bull.* **1979**, *14*, 1437.
(2) Diemann, E.; Müller, A. *Coord. Chem. Rev.* **1973**, *10*, 79.
(3) Chianelli, R. R.; Dines, M. B. *Inorg. Chem.* **1978**, *17*, 2758.
(4) Ratnasamy, P.; Rodrique, L.; Leonard, A. J. *J. Phys. Chem.* **1973**, *77*, 2242–2246.
(5) Diemann, E. *Z. Anorg. Allg. Chem.* **1977**, *432*, 127–135.
(6) Liang, K. S.; deNeufville, J. P.; Jacobson, A. J.; Chianelli, R. R.; Betts, F. *J. Non-Cryst. Solids* **1980**, *35–36*, 1249.
(7) Liang, K. S.; Cramer, S. P.; Johnston, D. C.; Chang, C. H.; Jacobson, A. J.; deNeufville, J. P.; Chianelli, R. R. *J. Non-Cryst. Solids* **1980**, *42*, 345.

0020-1669/84/1323-1215$01.50/0

been an effort to quantitate some of the screening effects critical for interpretation of EXAFS amplitudes from atoms beyond the first coordination sphere of the X-ray-absorbing atom.

Experimental Section

Sample Preparation. $(NH_4)_2MoS_4$ and $(NH_4)_2WS_4$ were prepared from aqueous ammonium paramolybdate and tungstic acid solutions, respectively, by treatment with gaseous H_2S.[8] $(NH_4)_2WSe_4$ was obtained from Alfa Products, and $(NH_4)_2MoSe_4$ was prepared by treatment of an aqueous ammonium paramolybdate solution with gaseous H_2Se. All of these tetrachalcidometalates were examined by X-ray diffraction and Fourier transform infrared absorption spectroscopy. The absence of metal–oxygen vibrational bands was used to check the purity of the starting materials before preparation of the trichalcides.

MoS_3 and WS_3 were prepared by thermal decomposition of the corresponding ammonium tetrachalcidometalates under an oxygen-free helium atmosphere.[2] The decomposition temperature used was 200 °C. $MoSe_3$ and WSe_3 were made by formic acid precipitation,[3] followed by heat treatment at temperatures of 270 and 220 °C, respectively. Elemental analysis of the trichalcides gave metal-to-chalcogen ratios of 1:3.01, 1:3.00, 1:3.30, and 1:2.94, respectively, for MoS_3, WS_3, $MoSe_3$, and WSe_3. Metal dichalcides were prepared by further decomposition at elevated temperatures, and they showed the expected elemental analyses and poorly crystalline X-ray diffraction patterns.[9]

All samples were kept sealed under nitrogen until recording the absorption spectra. However, during data collection the samples were exposed to air. Although the short-term stability of most of these samples was adequate, the $(NH_4)_2MoSe_4$ sample was found to be quite air sensitive. The more stable $(NH_4)_2MoO_2Se_2$ was synthesized by literature methods[10] and used as a standard instead.

Data Collection. The X-ray absorption spectra were recorded in the transmission mode at the Stanford Synchrotron Radiation Laboratory, using Si [220] crystal monochromators. The instruments were calibrated by using 20 003.9 eV for the Mo-foil edge inflection point and 10 204 eV for the W-foil L_{III} edge. Ionization chambers filled with argon gas were used as detectors for the molybdenum spectra, while nitrogen gas was used for the tungsten and selenium spectra.

Data Analysis

EXAFS is the observed modulation ($\Delta\mu$) of the absorption coefficient divided by the smoothly varying absorption coefficient (μ_0). An expression often used in the interpretation of EXAFS data is

$$\chi(\mathbf{k}) = \sum_b \frac{N_b|f_b(\pi,\mathbf{k})|}{\mathbf{k}R_{ab}^2} e^{-[2\sigma^2_{ab}k^2+R_{ab}/\lambda]} \sin [2\mathbf{k}R_{ab} + \alpha_{ab}(\mathbf{k})] \quad (1)$$

In this expression N_b is the number of back-scatterers at distance R_{ab} from the X-ray absorbing atom, $|f_b(\pi,\mathbf{k})|$ is the electron atom back-scattering amplitude, σ^2_{ab} is the mean square deviation for a Gaussian distribution of R_{ab}, $\alpha_{ab}(\mathbf{k})$ is the total phase shift, λ is the mean free path for the photoelectron, and $\mathbf{k}$ is the photoelectron wave vector.

Recently, there has been a growing appreciation that this equation overestimates EXAFS amplitudes, because multielectron excitations are ignored.[11-13] Similarly, there has never been much experimental justification for the simple mean free path expression, especially in light of the dramatic dependence of EXAFS amplitudes upon the nature and geometry of intervening atoms.[11-15] In this work the analysis is based on a revised expression:

$$\chi(\mathbf{k}) \cong \sum_b \frac{N_b[A_{ab}(\mathbf{k})]}{\mathbf{k}R_{ab}^2} [[T_i(\mathbf{k})]e^{-2\sigma^2_{ab}k^2}] \sin [2\mathbf{k}R_{ab} + \alpha_{ab}(\mathbf{k})] \quad (2)$$

In the above expression, the total amplitude function $A(\mathbf{k})$ has been designed to incorporate all amplitude effects except the presence of intervening atoms, which are accounted for by the screening function $T_i(\mathbf{k})$.

Numerically, there are two methods for obtaining $A(\mathbf{k})$ and $\alpha(\mathbf{k})$ from the experimental spectra. One approach is to use a complex Fourier transform[16] to obtain discrete values for the amplitude envelope and phase shift. An alternative procedure is to parameterize these functions and to refine the parameters by curve-fitting methods until a good fit to the experimental spectrum is obtained.[14] The second approach has been used in this work.

The MX_2 layer compounds were used for derivation of phase shifts for M (metal)–X (chalcogen) and M–M pairs. These phase shifts were then checked by predicting M–X distances in the corresponding $(NH_4)_2MX_4$ salts and comparing the EXAFS results with the crystallographic values. Derivation of $A(\mathbf{k})$ requires knowledge of not only N and R but σ^2 as well. Fortunately, the tetrahedral symmetry of the MX_4^{2-} ions makes calculation of their σ^2 particularly straightforward.[17] By using the calculated σ^2 to correct the observed amplitude for thermal motion, it was possible to determine a total amplitude function $A(\mathbf{k})$ for each M–X pair. The process was then reversed for calculation of σ^2 in other structures, by assuming $A(\mathbf{k})$ to be transferable and varying σ^2 for the best fit. The actual functions obtained are given in the supplementary material.

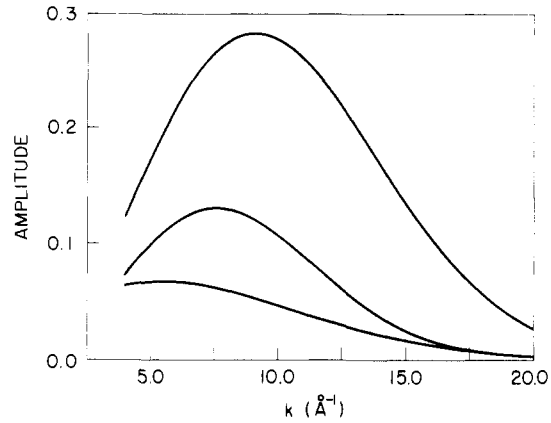

Figure 1. Overall Mo–Mo amplitudes for oxide- (top), sulfide- (middle), and selenide-bridged (bottom) compounds $K_2[Mo_3O_4(ox)_3(H_2O)_3]$, MoS_2, and $MoSe_2$. The amplitudes have been normalized for distance and coordination number but not Debye–Waller factors or screening effects.

Results

Intervening Atom Effects. When interpreting EXAFS amplitudes for back-scatterers beyond the first coordination sphere, the effects of intervening atoms have to be considered. In Figure 1 a Mo–Mo total amplitude derived from an oxo-bridged compound[18] is compared with sulfur-bridged and

(8) Müller, A.; Diemann, E. *Z. Naturforsch., B: Anorg. Chem., Org. Chem., Biochem., Biophys. Biol.* **1968**, *23B*, 1607.
(9) (a) Wildervanck, J. C.; Jellineck, F. *Z. Anorg. Allg. Chem.* **1964**, 328, 309–318. (b) Voorhoeve, R. J.; Wolters, H. *Ibid.* **1970**, *376*, 165–179.
(10) Müller, A.; Diemann, E. *Chem. Ber.* **1969**, *102*, 945.
(11) Eisenberger, P.; Lengeler, B. *Phys. Rev. B: Condens. Matter* **1980**, *22*, 3551–3562.
(12) Stern, E. A.; Bunker, B. A.; Heald, S. M. *Phys. Rev. B: Condens. Matter* **1980**, *21*, 5521–5539.
(13) Lee, P. A.; Citrin, P. H.; Eisenberger, P.; Kincaid, B. M. *Rev. Mod. Phys.* **1981**, *53*, 769.
(14) Cramer, S. P.; Hodgson, K. O.; Stiefel, E. I.; Newton, W. E. *J. Am. Chem. Soc.* **1978**, *100*, 2748–2761.
(15) Teo, B. K. *J. Am. Chem. Soc.* **1981**, *103*, 3990.
(16) Eisenberger, P.; Shulman, R. G.; Kincaid, B. M.; Brown, G. S.; Ogawa, S. *Nature (London)* **1978**, *274*, 30–34.
(17) Nagarajan, G. *Indian J. Pure Appl. Phys.* **1964**, *2*, 17–22.

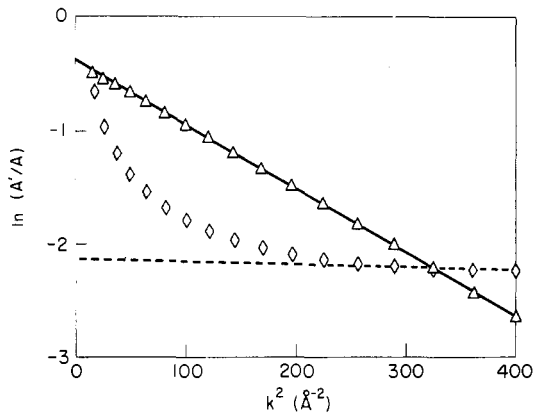

Figure 2. Logarithms of ratios of Mo–Mo amplitudes for oxide-, sulfide-, and selenide-bridged compounds: Δ, S-bridged/O-bridged, ◊, Se-bridged/O-bridged.

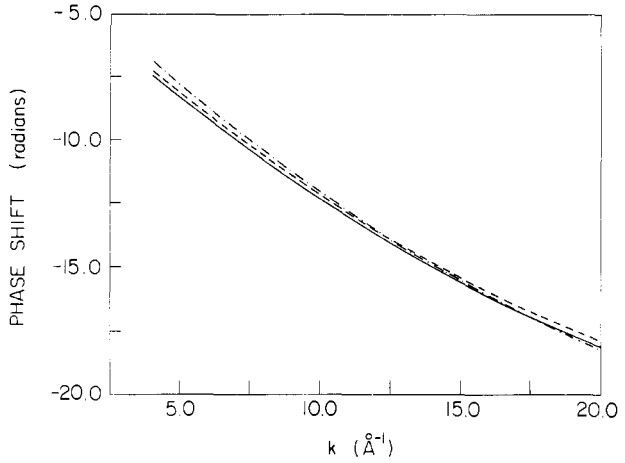

Figure 3. Mo–Mo phase shifts extracted from spectra of oxide- (---), sulfide- (—), and selenide-bridged (-·-) compounds. The same E_0 (200 25 eV) was used in all three cases.

selenium-bridged functions. These curves represent the product $[A_{ab}(\mathbf{k})][T_i(\mathbf{k})]\exp(-2\sigma^2_{ab}\mathbf{k}^2)$ in eq 2. Were the difference in amplitudes solely a matter of different Debye–Waller factors, a plot of the logarithm of their ratios vs. $\mathbf{k}^2$ (Figure 2) would exhibit straight lines intersecting at the origin.[19] This is not the case, however, indicating an amplitude reduction distinct from any Debye–Waller effect. For sulfur-bridged Mo–Mo amplitudes, the reduction relative to the oxo-bridged case is a nearly constant factor of 0.67. For selenium-bridged Mo–Mo amplitudes the reduction is **k** dependent, but an average value is 0.25. Both of these values were obtained by using the oxo-bridged Mo–Mo amplitude envelope with a variable σ and a variable scale factor to fit the MX_2 metal–metal EXAFS. Although a complete set of standard compounds was lacking for testing the analogous functions in chalcide-bridged tungsten EXAFS, a clear reduction in W–W amplitude was also observed in WSe_2 vs. WS_2.

In contrast with EXAFS amplitudes, Mo–Mo phase shifts proved to be relatively independent of the type of bridging atom. This is illustrated in Figure 3, where the three independently derived Mo–Mo phase shifts are shown to be nearly identical.

Standard Compounds. Table I summarizes the EXAFS results obtained on $(NH_4)_2MX_4$ and MX_2 materials. The

Table I. Summary of $(NH_4)_2MX_4$ and MX_2 Results

	M–X			M–M	
compd	R_{EXAFS}, Å	R_{xtal}, Å	σ, Å	R_{EXAFS}, Å	R_{xtal}, Å
$(NH_4)_2MoS_4$	2.19[a]	2.17[d]	0.0427[j]		
MoS_2	*b*	2.42[e]	0.057[a]	3.166[a]	3.160[e]
$(NH_4)_2MoO_2Se_2$	2.29[a]		0.0450[k]		
$MoSe_2$	*b*	2.49[f]	0.060[a]	3.289[a]	3.288[f]
$(NH_4)_2WS_4$	2.195[a]	2.165[g]	0.0452[j]		
WS_2	*b*	2.41[e]	0.061[a]	*b*	3.154[e]
$(NH_4)WSe_4$	2.30[a]	2.317[h]	0.0407[k]		
	2.30[c]	2.317[h]	0.0407[k]		
WSe_2	*b*	2.51[i]	0.056[a]	*b*	3.286[l]
	b	2.51[i]	0.058[c]		

[a] Calculated from Mo or W EXAFS. [b] Used as standard. [c] Calculated from Se EXAFS. [d] Reference 26. [e] Reference 27. [f] Reference 28. [g] Reference 29. [h] Reference 30. [i] Reference 32. [j] Calculated from vibrational spectrum.[17] [k] Calculated from vibrational spectrum (this work). [l] Reference 31.

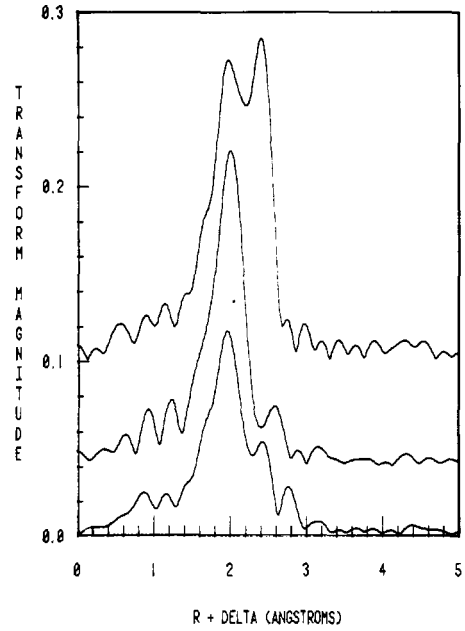

Figure 4. Comparison of the EXAFS Fourier transforms for MoS_3 (bottom), $(NH_4)_2[Mo_2(S_2)_6]$ (middle), and $(NH_4)_2[Mo_3S(S_2)_6]$ (top). Transform range: $\mathbf{k}$ = 4–18 Å^{-1}, $\mathbf{k}^3$ weighing.

MX_4^{2-} M–X bond length root-mean-square deviation (σ) obtained from the vibrational frequencies was always between 0.041 and 0.045 Å. The corresponding σ's obtained from the EXAFS of the MX_2 compounds were all between 0.056 and 0.061 Å. This confirms that systems with similar bonding have similar Debye–Waller factors. The distances calculated from the EXAFS spectra were all within 0.03 Å of those determined crystallographically.

Metal Trichalcide and Model Compound Fourier Transforms. Comparing the EXAFS Fourier transforms of the trichalcides with those of model compounds and the corresponding dichalcides is the simplest way to convey the structural results of this work. Figure 4 shows the EXAFS Fourier transforms of amorphous MoS_3 as well as crystalline $(NH_4)_2[Mo_2(S_2)_6]$ and $(NH_4)_2[Mo_3S(S_2)_6]$. It is seen that the Mo–S peak in the MoS_3 spectrum is less pronounced than in these model compounds, while the Mo–Mo peak is intermediate in intensity. Comparisons of Fourier-transformed EXAFS for the amorphous trichalcides and the crystalline dichalcides are shown in Figures 5 and 6. The metal–chalcogen peak in the trichalcide transforms is always significantly broader than the related feature in the dichalcide, and the metal–metal features are dramatically different. With the exception of MoS_3, no

(18) Cramer, S. P.; Eidem, P. K.; Dori, Z.; Gray, H. B. *J. Am. Chem. Soc.* **1983**, *105*, 799–802.
(19) Stern, E. A.; Sayers, D. E.; Lytle, F. W. *Phys. Rev. B: Solid State* **1975**, 4836.

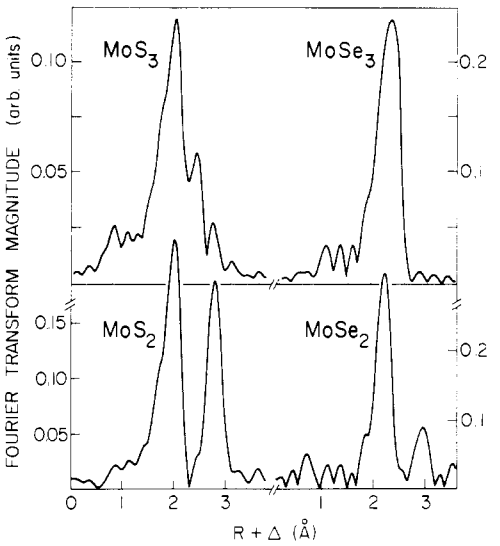

Figure 5. EXAFS Fourier transforms for MoS_2, MoS_3, $MoSe_2$, and $MoSe_3$. Transform range: $k = 4–20$ Å^{-1}, k^3 weighting. Note the difference in scales.

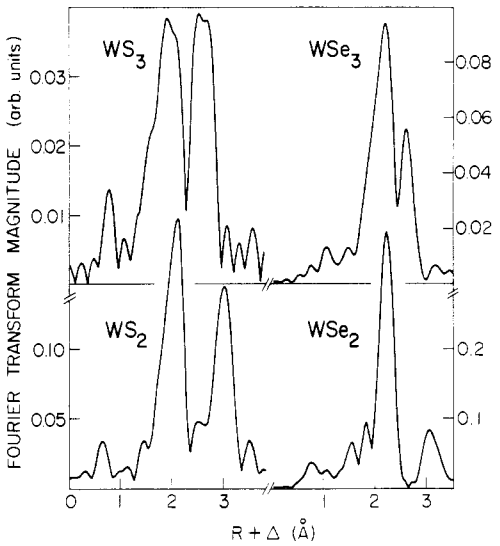

Figure 6. EXAFS Fourier transforms for WS_2, WS_3, WSe_2, and WSe_3. Transform range: $k = 4–16$ Å^{-1}, k^3 weighting. Again, note the difference in scales.

evidence is seen of the metal–metal interaction at about 3.2 Å which is characteristic of the dichalcides. Instead, evidence for a shorter metal–metal interaction can be clearly seen in the transforms for MoS_3, WS_3, and WSe_3, and it can be inferred from the broad peak of $MoSe_3$. Beyond 3.2 Å, the transforms of the trichalcides exhibit no significant features. Finally, the selenium-edge EXAFS Fourier transforms for $MoSe_3$ and WSe_3 showed only a single broad peak, as illustrated in Figure 7.

$NbSe_3$ Analysis. Because the trichalcides are amorphous, the possible effects of a large amount of static disorder on the accuracy of the EXAFS analysis are a concern.[20] For this reason, crystalline $NbSe_3$ was examined by using both Nb and Se EXAFS, with $NbSe_2$ as a standard (Figures 8 and 9). Despite the wide variation in Nb–Se distances in $NbSe_3$, the 2.678 Å distance calculated from the Nb EXAFS is within 0.01 Å of the crystallographic average. If it is assumed that the thermal contribution to σ in $NbSe_2$ and $NbSe_3$ is the same, then a value for the static contribution to σ of 0.091 Å can be derived from the Nb EXAFS. This compares extremely

(20) Eisenberger, P.; Brown, G. S. *Solid State Commun.* **1979**, *29*, 481–484.

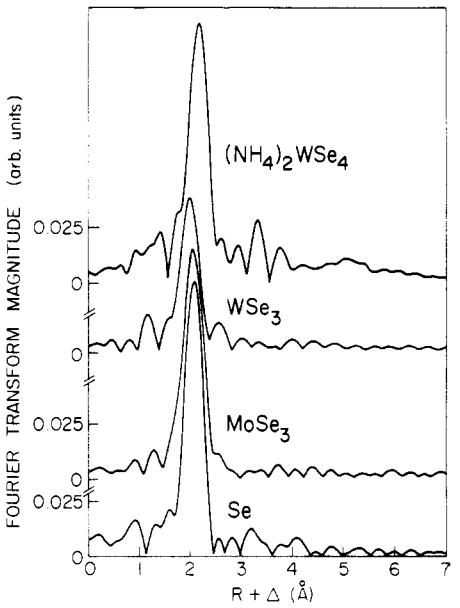

Figure 7. Se edge EXAFS Fourier transforms for several Se compounds. Transform range: $k = 4–16$ Å^{-1}, k^3 weighting.

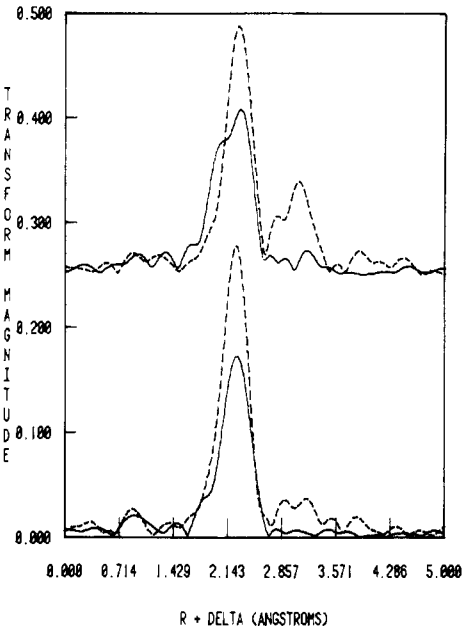

Figure 8. EXAFS Fourier transforms for $NbSe_2$ and $NbSe_3$. Top: dashed, $NbSe_2$ Se EXAFS; solid, $NbSe_3$ Se EXAFS. Bottom: dashed, $NbSe_2$ Nb EXAFS; solid, $NbSe_3$ Nb EXAFS. Se data have been multiplied by 2 and displaced vertically for clarity. Transform range: $k = 4–18$ Å^{-1}, k^3 weighting.

well with the static σ of 0.087 Å calculated from the crystal structure. Similar results were obtained from the Se EXAFS of this material.

MX_3 and Model Compound Curve Fitting. The best fits to the data using the metal EXAFS are shown in Figure 10, and Se EXAFS fits are shown in Figure 11. The results of the curve-fitting analyses are presented in Table II for MoS_3 and molybdenum-sulfur cluster model compounds and in Table III for all of the trichalcides. The most significant result from the model compound studies was the substantial variation in the root-mean-square amplitude (σ) calculated for the Mo–Mo distance. The smallest value (0.030 Å) was calculated for the triangular cluster $[Mo_3S(S_2)_6]^{2-}$. Significantly larger values of 0.047 and 0.069 Å were found for MoS_2 and $[Mo_2(S_2)_6]^{2-}$, respectively. This is in line with previous results for triangular oxo-bridged Mo clusters, where the σ of 0.031 Å found for

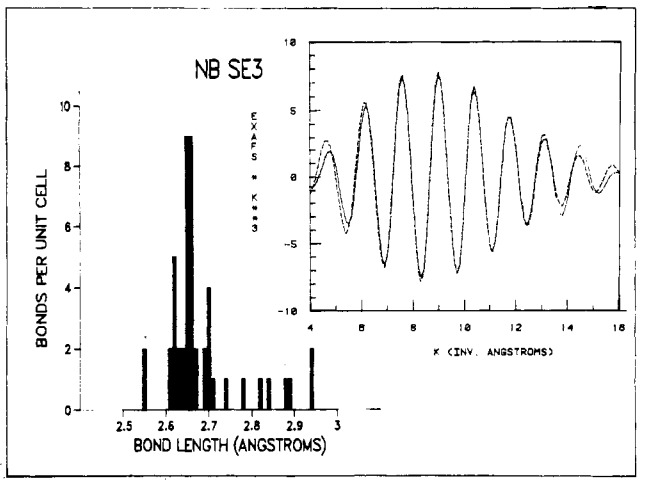

Figure 9. Curve-fitting analyses of $NbSe_3$ EXAFS using Nb EXAFS. Solid lines are filtered EXAFS data, dashed lines are best fit. Also shown is a histogram of Nb–Se distances in the unit cell of the crystal structure.

Table II. Mo-S Compound Results

		Mo-S			Mo-Mo		
structure		coord no.	R, Å	σ, Å	coord no.	R, Å	σ, Å
MoS_2	*a*	6	2.42[f]	0.057	6	3.166	0.061
	b	5.3	2.42	0.052	6.0	3.166	0.061
	c	6	2.42		6	3.160	
$[Mo_3S(S_2)_6]^{2-}$	*a*	7	2.43	0.072	2	2.726	0.030
	b	6.9	2.44	0.073	2.6	2.725	0.040
	d	7	2.433		2	2.722	
$[Mo_2(S_2)_6]^{2-}$	*a*	8	2.46	0.078	1	2.823	0.067
	b	6.7	2.46	0.070	0.9	2.827	0.061
	c	8	2.451		1	2.827	
MoS_3	*a*	6	2.44	0.085	1	2.746	0.054
					1	3.158	0.071
	b	5.5	2.44	0.082	1.5	2.745	0.064
					0.9	3.158	0.066

[a] Coordination numbers were held fixed; σ and R were calculated from EXAFS. [b] Coordination number, σ, and R all varied in EXAFS fit. [c] Reference 27. [d] Reference 32. [e] Reference 33. [f] Used as standard.

$[Mo_3O_4(ox)_3(H_2O)_3]^{2-}$ was significantly less than the 0.037–0.44 Å values found for dinuclear species.[18]

For MoS_3, when a single short Mo–Mo interaction was assumed, a distance of 2.75 Å and a σ of 0.054 Å were calculated. These values fall between the dinuclear and trinuclear Mo–S model compound results. A second Mo–Mo distance of 3.16 Å was also calculated, as well as an average Mo–S bond length of 2.44 Å. The fit residual was almost halved by using two different Mo–S distances separated by 0.1 Å rather than a single broad distribution. As discussed below, this might be expected in view of the presence of molybdenum sulfide and molybdenum disulfide bonds in this material. However, a unique determination of multiple Mo–S distances is not possible with the resolution and complexity of the current data.

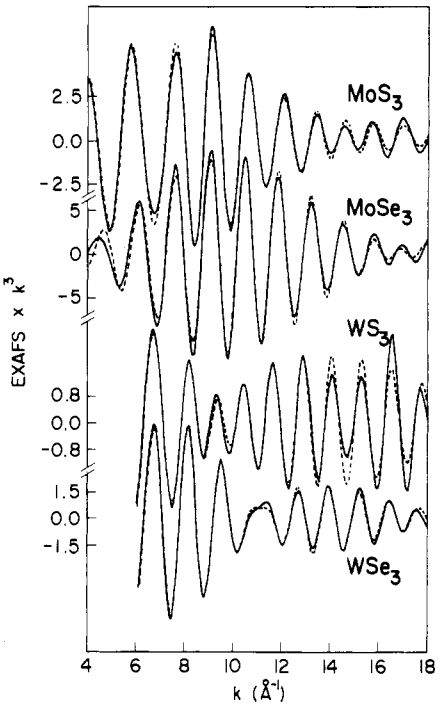

Figure 10. Best fits for the trichalcide EXAFS from the metal point of view (from top to bottom) of MoS_3, $MoSe_3$, WS_3, and WSe_3: (—) experimental data; (---) best fit.

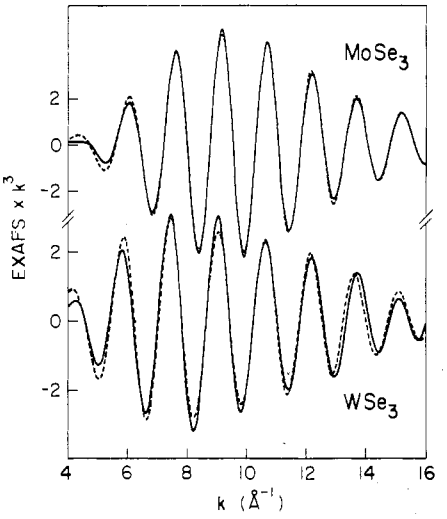

Figure 11. Best fits for the $MoSe_3$ and WSe_3 EXAFS from the selenium point of view: (—) experimental data; (---) best fit.

Table III. MX_3 Curve-Fitting Results[a]

		M-X or X-M			M-M		X-X	
compd		coord no. (±25%)	R, Å	σ, Å	coord no.	R, Å	coord no.	R, Å
MoS_3		6	2.44	0.082	1-2	2.75		
WS_3		8	2.41	0.14	1-2	2.75		
$MoSe_3$	Mo EXAFS	8	2.53	0.073	1-2	2.79		
	Se EXAFS	2	2.52	0.094			1-2	2.35
WSe_3	W EXAFS	8	2.55	0.11	1-2	2.77		
	Se EXAFS	2	2.58	0.12			1-2	2.37
$NbSe_3$	Nb EXAFS	7	2.68	0.091[c]				
	Se EXAFS	3	6.65				1.7	2.37
	X-ray diff[b]	8	2.683	0.087[d]				

[a] See text for discussion of statistical and systematic errors. [b] Reference 36. [c] Static σ (only), calculated from EXAFS. [d] Static σ (only), calculated from crystal structure.

In the EXAFS of WS_3, in contrast with MoS_3, only two components were required for a good fit, a W–S distance of 2.41 Å, and a W–W distance of 2.75 Å. The use of two different W–S distances did not improve the fit, nor was there a need for a second longer W–W distance. A better fit was obtained using eight rather than six sulfurs, and the W–W interaction number could be made as high as two. The σ of 0.13 Å calculated for the W–S distance distribution is significantly larger than the 0.057-Å value obtained for WS_2 or even the 0.086-Å value found for MoS_3.

For $MoSe_3$, although it is not resolved in the Fourier transform, a Mo–Mo distance of 2.79 Å was found by the fits, as well as an average Mo–Se bond length of 2.53 Å. From the Se EXAFS an independent value of 2.52 Å was obtained, as well as a Se–Se distance of 2.35 Å. As with MoS_3, the use of two discrete distributions of Mo–Se distances cut the residual in half. No evidence for a longer range Mo–Mo interaction could be found.

Finally, with WSe_3 a W–W interaction is clear in the Fourier transform, and curve fitting gave a W–W distance of 2.77 Å. A W–Se distance of 2.55 Å was calculated from the W EXAFS, and as with WS_3, a broad distribution (σ = 0.11 Å) gave the best fit. The Se EXAFS indicated W neighbors at a distance of 2.58 Å, also with a broad distribution (σ = 0.12 Å). Evidence for a short (2.37 Å) Se–Se distance was also found in the Se EXAFS.

Discussion and Conclusions

Accuracy of Results. At this point it is appropriate to discuss the potential sources of error for the values reported in Tables I–III. The first source to consider is the data itself. For the concentrated samples dealt with here, the noise due to electronics and photon statistics can be neglected and the primary concern is possible EXAFS amplitude reductions caused by sample inhomogeneity and beam harmonics. As discussed by Stern,[12] all of these effects are minimized by using relatively thin samples. Accordingly, samples with optical densities above the edge of less than 1 have been used, and a reproducibility of EXAFS amplitudes of better than ±5% was found.

A more important consideration in the determination of coordination numbers is the assumption of transferability of the amplitude functions $A(\mathbf{k})$ and the transmission functions $T(\mathbf{k})$. From work with the Mo–S model compounds it is estimated that $A(\mathbf{k})$ is transferable to about ±10%. However, the transferability of $T(\mathbf{k})$ has not been rigorously tested; such an investigation is beyond the scope of this work. In fact, if the M–X–M angle approached 180°, it is known that multiple scattering effects would strongly affect the EXAFS amplitude.[15] Accordingly, extreme caution should be used in interpreting amplitudes beyond the first coordination sphere. The second-shell coordination numbers have deliberately been left imprecise, and Debye–Waller factors have not been quoted at this time.

Even within the first coordination sphere, interpretation of coordination numbers is complicated by the correlation between the Debye–Waller factor σ and the coordination number N. Assuming too large a value for N will be compensated for by a larger σ, while too small a value for N will yield a lower value for σ. This correlation between N and σ introduces an uncertainty that depends on the range and quality of the data. It is estimated that the combined amplitude errors involved are on the order of ±25%. For the MX_3 results this means that MoS_3 most likely has between 5- and 7-coordinate molybdenum, while the remaining trichalcides have 6–10-coordinate metals. The upper values in this range are probably chemically unreasonable.

Two sources of error should be considered in regard to the distance determinations. The first is the assumption used here of phase shift transferability. The results presented in Figure 3, as well as the success of numerous structure predictions such as in Tables I–III, validate this assumption to about ±0.02-Å accuracy. A more subtle source of error involves the effects of non-Gaussian distributions. As discussed by Eisenberger and Brown,[20] if the radial distribution function tails asymmetrically toward longer distances, the EXAFS method will underestimate the true average distance. To account for such effects, DeCrescenzi et al. used a modified expression to model the EXAFS.[21] Their asymmetry parameter σ_D was incorporated into the current curve-fitting analyses, but no significant improvement in the fits was obtained. Finally, it is noted that even a symmetric Gaussian distribution requires a phase shift correction if σ is different from the model used. This may result is a slight underestimation of the average M–X bond length in the MX_3 materials.

Proposed Local Structure for MX_3 Materials. The nature of the amorphous trichalcides has been the subject of several previous studies,[4-7,22] and four distinct structural models have been proposed. The earliest proposal based on X-ray scattering by Ratnasamy et al.[4] was for an "immediate environment (within 6 Å) of both the Mo^{4+} and S^{2-} ions...not much different from that in hexagonal MoS_2". In essence, these authors envisaged a random arrangement of small fragments of MoS_2 layers. A subsequent ESCA study by Stevens and Edmonds[22] proposed "an intimate association of subcrystalline MoS_2 and amorphous sulfur". Later, from X-ray radial distribution results Diemann[5] proposed a structure based upon "microcrystallites which contain three metal atoms and are bridged statistically to each other". The latter model was based on analogy with the structure of the $W_3S_9^{2-}$ anion.[23] Finally, Liang et al.[6] proposed a chainlike structure for MoS_3 on the basis of high-resolution X-ray radial distribution function data and ESCA studies. This proposed structure is analogous to the crystalline trichalcides of neighboring groups 4 and 5 such as NbS_3. The current EXAFS results for MoS_3 can unambiguously rule out the first two models. They also differ quantitatively from the model proposed by Diemann,[5] who suggested longer metal–metal distances of 2.91 Å.

The 2.75-Å Mo–Mo distance can be accounted for by invoking Mo–Mo bonding, which implies that the molybdenum has been partially reduced and the sulfur has been partially oxidized. Evidence for this also comes from XPS studies[6] that indicate the presence of S_2^{2-} in the S_2^{2-}:S^{2-} ratio of 0.5:2. Finally, a S–S stretching mode has also been identified in the infrared spectrum.[7] All of the EXAFS, IR, XPS, and RDF data are therefore consistent with the chain structure proposed on the basis of a repeating $Mo_2(S^{2-})_4(S_2^{2-})$ unit.[6]

The exact local geometric arrangement of atoms in the other MX_3 materials is impossible to determine from EXAFS alone, but as a working model, structure I is useful to consider. Triple

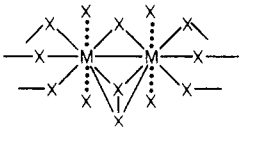

I

bridges are common in molybdenum and tungsten chemistry. The chalcide ions at the ends of structure I are assumed to bridge to other metal ions. The central bridging chalcide and dichalcide may also interact with other metals. One reason for placing the dichalcide across the metal–metal bond is analogy with known complexes such as $[W_2Cl_8Se(Se_2)]^{2-}$[24]

(21) DeCrescenzi, M.; Balzarotti, A.; Comin, F.; Incoccia, L.; Mobilio, S.; Motta, N. *Solid State Commun.* **1981**, *37*, 921–923.
(22) Stevens, G. C.; Edmonds, T. *J. Catal.* **1975**, *37*, 544–547.
(23) Koniger-Ahlborn, E.; Müller, A. *Angew. Chem.* **1975**, *87*, 598.
(24) Drew, M. G. B.; Fowles; G. W. A.; Page, E. M.; Rice, D. A. *J. Am. Chem. Soc.* **1979**, *101*, 5827.

and $Nb_2Br_4S_3$.[25] However, there remains the possibility that the random placement of this particular bond contributes to the amorphous nature of these materials.

One of the important conclusions reached from the systematic studies of EXAFS amplitudes was the large variability in amplitude for bridged neighbors. Accordingly, any modeling of the local structure of these materials should consider structures in which each metal has on the average more than one bridged metal neighbor. The simplest extensions are the trinuclear structures of either chainlike or cyclic form:

II III

In II the average metal-metal coordination from an EXAFS point of view would rise to $1^1/_3$, while structure III would show an average of 2 metal-metal interactions. Lengthening the former chainlike structure would raise the average metal-metal coordination asymptotically to 2. Examples of II and III such as $W_3S_9^{2-}$ and $[Mo_3S(S_2)_6]^{2-}$ are also well documented in the literature.

The dramatic spectral differences between MoS_3 and $[Mo_3S(S_2)_6]^{2-}$ rule out the presence of a significant number of triangular trinuclear clusters in MoS_3, as does the XPS data.[6] However, for the other MX_3 materials the relative distribution of dinuclear and trinuclear sites is not clear from the EXAFS and is probably better addressed by X-ray radial distribution function analysis and other studies. An important point about the trinuclear species is that they imply further reduction of the metal to provide electrons for the additional metal-metal bonds. Accordingly, for M^{4+} the stoichiometry becomes $(M^{4+})(X^{2-})(X_2^{2-})$, while for M^{3+} one could write the electronic distribution as $(M^{3+})(X_2^{2-})_{3/2}$. It is certainly possible that extensive electron delocalization makes a detailed assignment of formal oxidation states impossible and also contributes to the interesting properties of these materials.

Acknowledgment. Sue Rich and Dr. Wie-Hin Pan are thanked for their assistance in the preparation of the compounds used in this study. We also thank the staff of SSRL for their assistance in facilitating our experiments.

Registry No. MoS_3, 12033-29-3; WS_3, 12125-19-8; $MoSe_3$, 12033-30-6; WSe_3, 88981-34-4.

Supplementary Material Available: Listings of the raw EXAFS data as well as the parameterized phase shift and amplitude functions used and/or derived in this work (65 pages). Ordering information is given on any current masthead page.

(25) Drew, M. G. B.; Baba, I. B.; Rice, D. A.; Williams, D. M. *Inorg. Chim. Acta* **1980**, *44*, L217-L218.
(26) Schäfer, H.; Schäfer, G.; Weiss, A. *Z. Naturforsch., B: Anorg. Chem., Org. Chem., Biochem., Biophys., Biol.* **1964**, *19B*, 76.
(27) Dickinson, R. G.; Pauling, L. *J. Am. Chem. Soc.* **1923**, *45*, 1466.
(28) James, P. B.; Lavik, M. T. *Acta Crystallogr.* **1963**, *16*, 1183.
(29) Sasvari, K. *Acta. Crystallogr.* **1963**, *16*, 719-724.
(30) Müller, A.; Krebs, B.; Beyer, H. *Z. Naturforsch., B: Anorg. Chem., Org. Chem., Biochem., Biophys., Biol.* **1968**, *23B*, 1537-1538.
(31) Gamble, F. R. *J. Solid State Chem.* **1974**, *9*, 358-367.
(32) Müller, A.; Pohl, S.; Dartmann, M.; Cohen, J. P.; Bennett, J. M.; Kirchner, R. M. *Z. Naturforsch., B: Anorg. Chem., Org. Chem.* **1979**, *B34*, 434-436.
(33) Müller, A.; Nolte, W. O.; Krebs, B. *Angew. Chem., Int. Ed. Engl.* **1978**, *17*, 279-280.
(34) Meerschaut, A.; Rouxel, J. *J. Less-Common Met.* **1975**, *39*, 197-203, 39.

Contribution from the Laboratoire de Physicochimie des Solides, Université de Nantes, 44072 Nantes Cedex, France, and Department of Chemistry, North Carolina State University, Raleigh, North Carolina 27650

Electronic Structures of Transition-Metal Tetrachalcogenides $(MSe_4)_nI$ (M = Nb, Ta)

PASCAL GRESSIER,[1a] MYUNG-HWAN WHANGBO,*[1b,c] ALAIN MEERSCHAUT,[1a] and JEAN ROUXEL[1a]

Received July 22, 1983

Transition-metal tetraselenides $(MSe_4)_nI$ (M = Nb, Ta) contain MSe_4 chains with varying degrees of band filling. Tight-binding calculations were performed on various MSe_4 chains to probe how one-dimensional phenomena such as Peierls distortion and charge density wave formation are affected by band filling. It is found that the d_{z^2} band of an MSe_4 chain is well separated from other bands and the effect of the interchain Se···Se interaction upon the d_{z^2} band is appreciable only for those wave vectors along the chain direction $\Gamma \rightarrow Z$. The driving force for metal ion distortion along the MSe_4 chains is found to sharply diminish as the d_{z^2} band filling decreases from $^1/_2$.

In connection with low-dimensional phenomena such as Peierls distortion[2] and sliding charge density wave (CDW),[3] a new series of transition-metal tetrachalogenides $(MX_4)_nY$ (M = Nb, Ta; X = S, Se; Y = halogen) have recently been synthesized.[4] These compounds consist of MX_4 chains, which are parallel and well separated from one another by halogen atoms. This provides a pseudo-one-dimensional character to those compounds. In each MX_4 chain, a metal atom M is sandwiched by two nearly rectangular X_4 units as indicated in **1**. Any two adjacent X_4 units of **1** make a dihedral angle

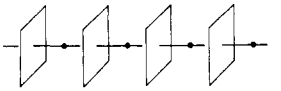

1

of almost 45°, and so a metal atom is located at the center of a rectangular antiprism of eight X atoms. For simplicity, the MX_4 chain **1** may be represented by **2**, where the heavy

2

dots refer to metal atoms M and the parallel lines perpendicular to the chain axis refer to X_4 units. **2** represents an ideal structure in which all the metal atoms are separated by the average M-M distance of *d*.

(1) (a) Université de Nantes. (b) North Carolina State University. (c) Camille and Henry Dreyfus Teacher-Scholar (1980-1985).
(2) (a) Peierls, R. E. "Quantum Theory of Solids"; Oxford University, Press: London, 1955; p 108. (b) Whangbo, M.-H. *Acc. Chem. Res.* **1983**, *16*, 95.
(3) (a) Berlinsky, A. J. *Contemp. Phys.* **1976**, *17*, 331. (b) DiSalvo, F. J. "Electron-Phonon Interactions"; Riste, T., Ed.; Plenum Press: New York, 1977; p 107. (c) White, R. M.; Geballe, T. H. "Long Range Order in Solids"; Academic Press: New York, 1979.
(4) (a) Gressier, P.; Meerschaut, A.; Guémas, L.; Rouxel, J.; Monceau, P. *J. Solid State Chem.* **1984**, *51*, 141. (b) Meerschaut, A.; Palvadeau, P.; Rouxel, J. *J. Solid State Chem.* **1977**, *20*, 21. (c) Guémas, L.; Gressier, P.; Meerschaut, A.; Louër, D.; Grandjean, D. *Rev. Chim. Miner.* **1981**, *18*, 91. (d) Gressier, P.; Guémas, L.; Meerschaut, A. *Acta Crystallogr. Sect. B: Struct. Crystallogr. Cryst. Chem.* **1982**, *38*, 2877. (e) Meerschaut, A.; Gressier, P.; Guémas, L.; Rouxel, J. *J. Solid State Chem.* **1984**, *51*, 307.

0020-1669/84/1323-1221$01.50/0